Supplemental materials

Kei Yamamoto,[1,2,*] Weichao Yu,[3] Tao Yu,[4] Jorge Puebla,[2] Mingran Xu,[2,5] Sadamichi Maekawa,[2,6,1] and Gerrit Bauer[3,7]

[1]*Advanced Science Research Center, Japan Atomic Energy Agency, Tokai 319-1195, Japan*
[2]*CEMS, RIKEN, Saitama, 351-0198, Japan*
[3]*Institute for Materials Research, Tohoku University, Sendai 980-8577, Japan*
[4]*Max Planck Institute for the Structure and Dynamics of Matter, 22761 Hamburg, Germany*
[5]*Institute for Solid State Physics, University of Tokyo, 5-1-5 Kashiwanoha, Kashiwa, Chiba 277-8581, Japan*
[6]*Kavli Institute for Theoretical Sciences, University of Chinese Academy of Sciences, Beijing 100049, People's Republic of China*
[7]*Advanced Institute for Materials Research, Tohoku University, Sendai 980-8577, Japan*

(Dated: September 17, 2020)

CONTENTS

I. Linearisation and extension to wire geometry 1

II. Mode expansion 2

III. Rayleigh SAW amplitude 5

IV. Numerical Simulation 6

I. LINEARISATION AND EXTENSION TO WIRE GEOMETRY

We consider a slab of non-magnetic elastic body with thickness L_z and width L_x, on which a slab of ferromagnetic with thickness $d \ll L_z$ and width w is attached. Both are assumed infinitely extended in the y direction and dynamics uniform in y is considered. Our model is based on the phenomenological total free energy $E = W + F + I$ where W, F are the magnetic and elastic energies respectively and I is the interaction energy between $\boldsymbol{M}$ and $\boldsymbol{u}$. We take

$$W = \int d\boldsymbol{r} \left\{ -\mu_0 \boldsymbol{M} \cdot (\boldsymbol{H} + \boldsymbol{h}) - \frac{A}{2} \boldsymbol{n} \cdot \nabla^2 \boldsymbol{n} + \frac{\mu_0 M_s^2}{8\pi} \int d\boldsymbol{r}' \left(\boldsymbol{n} \cdot \nabla\right) \left(\boldsymbol{n}' \cdot \nabla'\right) \frac{1}{|\boldsymbol{r} - \boldsymbol{r}'|} \right\}, \tag{S.1}$$

$$F = \rho \int d\boldsymbol{r} \left\{ \frac{c_P^2 - 2c_S^2}{2} \left(\epsilon_{xx} + \epsilon_{yy} + \epsilon_{zz}\right)^2 + c_S^2 \left(\epsilon_{xx}^2 + \epsilon_{yy}^2 + \epsilon_{zz}^2 + 2\epsilon_{xy}^2 + 2\epsilon_{yz}^2 + 2\epsilon_{zx}^2\right) \right\}, \tag{S.2}$$

$$\begin{aligned} I = \int d\boldsymbol{r} \Big[& b_1 \left(\epsilon_{xx} n_x^2 + \epsilon_{yy} n_y^2 + \epsilon_{zz} n_z^2\right) + 2b_2 \left(\epsilon_{xy} n_x n_y + \epsilon_{yz} n_y n_z + \epsilon_{zx} n_z n_x\right) \\ & + \mu_0 M_s^2 \left\{ (1 - N_\perp) n_x \left(n_z \omega_{zx} + n_y \omega_{yx}\right) + N_\perp n_z \left(n_x \omega_{xz} + n_y \omega_{yz}\right) \right\} \Big], \end{aligned} \tag{S.3}$$

where $N_\perp = w/(w + d)$ is the demagnetising factor of the magnetic slab. In the main text, we focused on the case of an infinite film $L_x = w \to \infty$. Here we also include another limiting case of narrow wire $w \ll L_x$ as the two cases can readily be discussed in parallel (see Fig. S1).

We begin by writing down the linearised version of Eqs. (1) and (2) in the main text, which are derived from the free energy functional above by a variational principle:

$$\begin{pmatrix} -H_\parallel + i\alpha\omega/\mu_0|\gamma| & i\omega/\mu_0\,|\gamma| \\ -i\omega/\mu_0\,|\gamma| & -H_\perp + i\alpha\omega/\mu_0|\gamma| \end{pmatrix} \begin{pmatrix} n_\parallel \\ n_\perp \end{pmatrix} = -\frac{\gamma}{|\gamma|} \left(\boldsymbol{h} + \boldsymbol{h}_{\rm eff}\right), \tag{S.4}$$

$$\rho \left\{ \left(\omega^2 + c_S^2 \nabla^2\right) \boldsymbol{u} + \left(c_P^2 - c_S^2\right) \begin{pmatrix} \partial_x \\ 0 \\ \partial_z \end{pmatrix} (\partial_x u_x + \partial_z u_z) \right\} = -\boldsymbol{f} - \boldsymbol{f}_{\rm eff}, \tag{S.5}$$

* yamamoto.kei@jaea.go.jp

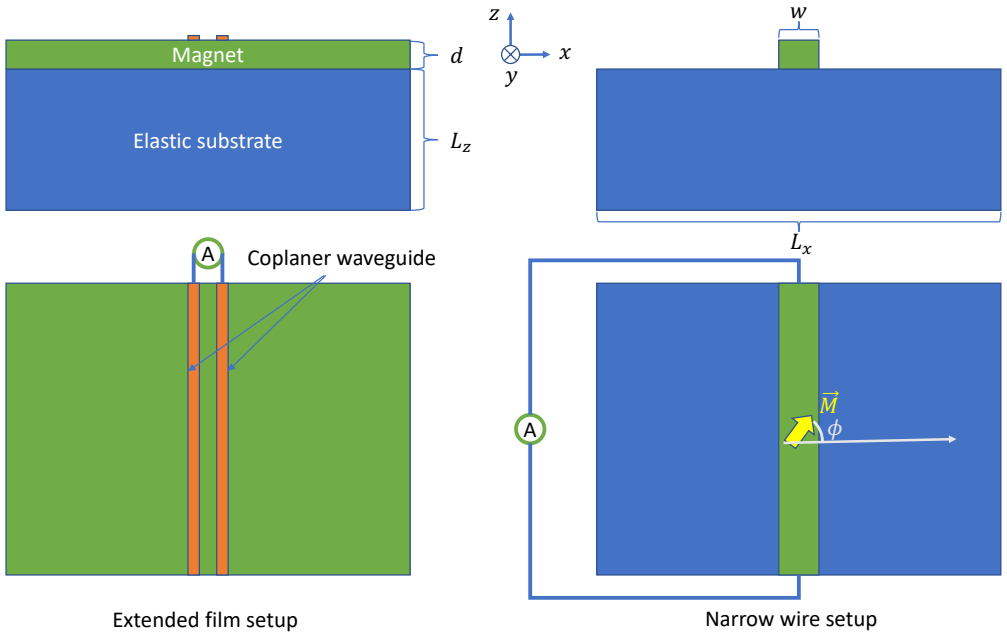

FIG. S1. Schematics of the film geometry (left) and wire geometry (right) considered in the supplementary materials.

where the normalised spin vector $\boldsymbol{n}$ has been expanded as

$$\boldsymbol{n} \approx \begin{pmatrix} \cos\theta \\ \sin\theta \\ 0 \end{pmatrix}\left(1 - \frac{n_\parallel^2 + n_\perp^2}{2}\right) + n_\parallel \begin{pmatrix} -\sin\theta \\ \cos\theta \\ 0 \end{pmatrix} + n_\perp \begin{pmatrix} 0 \\ 0 \\ 1 \end{pmatrix}, \tag{S.6}$$

and the Fourier transform in time has been applied. The internal fields $H_{\parallel,\perp}$ take different forms for the film and wire:

$$H_\parallel = \begin{cases} H - \frac{A}{\mu_0 M_s}\partial_x^2 + M_s\left(1 - N_k\right)\sin^2\theta & \text{film} \\ H\left|\cos\left(\theta - \phi\right)\right| + M_s\left(1 - N_\perp\right)\sin^2\theta & \text{wire} \end{cases}, \quad H_\perp = \begin{cases} H - \frac{A}{\mu_0 M_s}\partial_x^2 + M_s N_k & \text{film} \\ H\left|\cos\left(\theta - \phi\right)\right| + M_s N_\perp & \text{wire} \end{cases}. \tag{S.7}$$

Note $N_\perp = 1$ for film by definition, and for wire in general $\phi \neq \theta$ due to the in-plane shape anisotropy. The linearised effective forces are given by

$$\boldsymbol{h}_{\text{eff}} = -\frac{\gamma/|\gamma|}{\mu_0 M_s}\begin{pmatrix} -2b_1\epsilon_{xx}\cos\phi\sin\phi + \left\{2b_2\epsilon_{xy} - \left(1 - N_\perp\right)\omega_{xy}\right\}\left(\cos^2\phi - \sin^2\phi\right) \\ 2b_2\left(\epsilon_{zx}\cos\phi + \epsilon_{zy}\sin\phi\right) - N_\perp\omega_{zy}\sin\phi - \left(2N_\perp - 1\right)\omega_{zx}\cos\phi \end{pmatrix}, \tag{S.8}$$

$$\boldsymbol{f}_{\text{eff}} = \hat{\partial}_x\begin{pmatrix} -2b_1 n_\parallel\cos\phi\sin\phi \\ \left\{b_2 + \mu_0 M_s^2\left(1 - N_\perp\right)/2\right\} n_\parallel\left(\cos^2\phi - \sin^2\phi\right) \\ \left\{b_2 - \mu_0 M_s^2\left(2N_\perp - 1\right)/2\right\} n_\perp\cos\phi \end{pmatrix} + \hat{\partial}_z\begin{pmatrix} \left\{b_2 + \mu_0 M_s^2\left(2N_\perp - 1\right)/2\right\}\cos\phi \\ \left(b_2 + \mu_0 M_s^2 N_\perp/2\right)\sin\phi \\ 0 \end{pmatrix} n_\perp, \tag{S.9}$$

where $\hat{\partial}_x = \partial_x - \delta\left(x - w/2\right) + \delta\left(x + w/2\right)$. The delta functions in $\boldsymbol{f}_{\text{eff}} = -\delta I/\delta\boldsymbol{u}$ arise from the boundary terms when taking the variation of I with respect to $\boldsymbol{u}$. Therefore, omitting them would lead to non-conservation of energy at the boundaries. Although they could have been regarded as additional boundary conditions, that would have resulted in discussing modifications to the spatial profile of SAWs. As this task appears to be complicated if not intractable, and distracts attentions from the essential physics, we opt for an approximation scheme established in Ref. 6 of the main text.

II. MODE EXPANSION

We expand the full solutions of Eqs. (S.4) and (S.5) in terms of the individual solutions for Eq. (S.4) with $\boldsymbol{h}_{\text{eff}} = 0$ and Eq. (S.5) with $\boldsymbol{f}_{\text{eff}}$. In doing so for $n_{\parallel,\perp}$, we assume the film is sufficiently thin, i.e. $(d/2\pi)^2 < A/\mu_0 M_s^2$, so that the spin wave

modes are quantised along the thickness direction and all but the lowest frequency band may be disregarded. For YIG, the condition translates to roughly $d < 100$ nm. For films, the in-plane wavenumber k is a conserved quantity, which makes it possible to focus on one spin wave mode only in the expansion. For wires, if $w \gg 100$ nm, many spin wave modes with different k have to be retained in the expansion. To avoid this complication, we also assume $w < 100$ nm so that the expansion contains only the Kittel mode.

The expansion of $\boldsymbol{u}$ is common to the film and wire geometries. We impose the free-surface boundary conditions $\left(c_P^2 - 2c_S^2\right)\epsilon_{xx} + c_S^2\epsilon_{zz} = 0, \epsilon_{xz} = \epsilon_{yz} = 0$ at $z = d/2$, while the limit $L_z \to \infty$ is understood in order to ignore the boundary conditions on that surface. L_x is also assumed large so that Fourier transform in x is meaningful. There are four types of modes: a longitudinal mode (primary wave) $\boldsymbol{v}_{P,k,k_z}$ with velocity c_P, two transverse modes (secondary wave) $\boldsymbol{v}_{S,k,k_z}, \boldsymbol{v}_{T,k,k_z}$ with velocity c_S, and one surface (Rayleigh) mode $\boldsymbol{v}_{R,k}$ with velocity c_R. Note that the bulk modes (P,S,T) have the additional label $k_z > 0$ and the surface sound velocity c_R is determined by solving

$$\left(\frac{c_R}{c_S}\right)^3 - 8\left(\frac{c_R}{c_S}\right)^2 + 8\left\{3 - 2\left(\frac{c_S}{c_P}\right)^2\right\}\frac{c_R}{c_S} - 16\left\{1 - \left(\frac{c_S}{c_P}\right)^2\right\} = 0. \tag{S.10}$$

The general deformation $\boldsymbol{u}$ satisfying the free-surface boundary conditions can be expanded as

$$\boldsymbol{u} = \sum_k \left\{\sum_{k_z}\left(\beta_{P,k,k_z}\boldsymbol{v}_{P,k,k_z} + \beta_{S,k,k_z}\boldsymbol{v}_{S,k,k_z} + \beta_{T,k,k_z}\boldsymbol{v}_{T,k,k_z}\right) + \beta_{R,k}\boldsymbol{v}_{R,k}\right\} e^{ikx}, \tag{S.11}$$

where the coefficients $\beta_{P,k,k_z}, \beta_{S,k,k_z}, \beta_{T,k,k_z}, \beta_{R,k}$ are the amplitudes of respective modes to be determined, and the mode functions read

$$\boldsymbol{v}_{P,k,k_z} = A_+^P\begin{pmatrix}1\\0\\k_z/k\end{pmatrix}e^{ik_z(z-d/2)} + A_-^P\begin{pmatrix}1\\0\\-k_z/k\end{pmatrix}e^{-ik_z(z-d/2)} + A^S\begin{pmatrix}-i(k_S/k)\sin k_S\,(z-d/2)\\0\\\cos k_S\,(z-d/2)\end{pmatrix}, \tag{S.12}$$

$$\boldsymbol{v}_{S,k,k_z} = \frac{1}{N_S}\begin{pmatrix}-(k_z/k)\cos k_z\,(z-d/2)\\0\\i\sin k_z\,(z-d/2)\end{pmatrix}, \quad \boldsymbol{v}_{R,k,k_z} = \frac{1}{N_T}\begin{pmatrix}0\\1\\0\end{pmatrix}\cos k_z\left(z - \frac{d}{2}\right), \tag{S.13}$$

$$\boldsymbol{v}_{R,k} = \frac{1}{N_R}\begin{pmatrix}\left(1-\xi_S^2\right)\left\{e^{\kappa_P(z-d/2)} - \left(1-\xi_S^2\right)e^{\kappa_S(z-d/2)}\right\}\\0\\-i\sqrt{1-\xi_P^2}\left\{\left(1-\xi_S^2\right)e^{\kappa_P(z-d/2)} - e^{\kappa_S(z-d/2)}\right\}\operatorname{sgn}(k)\end{pmatrix}. \tag{S.14}$$

We introduced the notations

$$k_S = \sqrt{\frac{c_P^2k_z^2 + \left(c_P^2 - c_S^2\right)k^2}{c_S^2}}, \quad \xi_S^2 = \frac{c_R^2}{2c_T^2}, \quad \xi_P^2 = \frac{c_R^2}{c_P^2}, \quad \kappa_{P,S} = |k|\sqrt{1 - \frac{c_R^2}{c_{P,S}^2}}, \tag{S.15}$$

and the coefficients $A_\pm^P, A^S$ for the longitudinal mode satisfy

$$c_S^2 kk_z\left(A_+^P - A_-^P\right) = \left\{c_P^2k_z^2 + \left(c_P^2 - 2c_S^2\right)k^2\right\}A^S, \tag{S.16}$$

$$c_S^2\left\{c_P^2k_z^2 + \left(c_P^2 - 2c_S^2\right)k^2\right\}\left(A_+^P + A_-^P\right) = 2\left[c_P^2\left(c_P^2 - 2c_S^2\right)k_z^2 + \left\{\left(c_P^2 - 2c_S^2\right)^2 - 2c_S^4\right\}k^2\right\}A^S. \tag{S.17}$$

We further normalise the mode functions by

$$\frac{1}{L_z}\int_{-L_z-d/2}^{d/2} dz\left|\boldsymbol{v}_\mu\right|^2 = 1, \quad \mu = (P,k,k_z), (S,k,k_z), (T,k,k_z), (R,k). \tag{S.18}$$

In the limit $L_z \to \infty$, this amounts to

$$|N_S|^2 = \frac{k^2 + k_z^2}{2k^2}, \quad |N_T|^2 = \frac{1}{2}, \quad |N_R|^2 = \frac{1}{|k|L_z}\left\{\frac{\left(1-\xi_S^2\right)^2\left(2-\xi_P^2\right)}{2\sqrt{1-\xi_P^2}} + \frac{\left(1-\xi_S^2\right)^4 + 1 - \xi_P^2}{2\sqrt{1-2\xi_S^2}} - 2\left(1-\xi_S^2\right)\frac{\left(1-\xi_S^2\right)^2 + 1 - \xi_P^2}{\sqrt{1-\xi_P^2} + \sqrt{1-2\xi_S^2}}\right\}. \tag{S.19}$$

The behaviour $|N_R|^2 \to 0$ as $L_z \to \infty$ is not unphysical: The spurious L_z dependence turns out to disappear in the final expressions for observable quantities, as demonstrated shortly. The normalisation of $\boldsymbol{v}_{P,k,k_z}$ similarly fixes $A_\pm^P, A^S$, and although they are too tedious to be written down here, they converge to constants of order unity for $L_z \to \infty$ like the other bulk modes.

Let $\epsilon^{\mu}_{ij} = \{\partial_j(\boldsymbol{v}_\mu)_i + \partial_i(\boldsymbol{v}_\mu)_j\}/2, \omega^{\mu}_{ij} = \{\partial_j(\boldsymbol{v}_\mu)_i - \partial_i(\boldsymbol{v}_\mu)_j\}/2$ be the strain and rotation tensor components of the eigenmodes labelled by $\mu = (P,k,k_z),(S,k,k_z),(T,k,k_z),(R,k)$. Substituting Eq. (S.11) into Eq. (S.8) yields

$$\boldsymbol{h}_{\text{eff}} = -\frac{\gamma/|\gamma|}{\mu_0 M_s}\sum_{\mu}\beta_\mu \begin{pmatrix} -2b_1\epsilon^{\mu}_{xx}\cos\phi\sin\phi + \left\{2b_2\epsilon^{\mu}_{xy} - (1-N_\perp)\,\omega^{\mu}_{xy}\right\}\left(\cos^2\phi - \sin^2\phi\right) \\ 2b_2\left(\epsilon^{\mu}_{zx}\cos\phi + \epsilon^{\mu}_{zy}\sin\phi\right) - N_\perp\omega^{\mu}_{zy}\sin\phi - (2N_\perp - 1)\,\omega^{\mu}_{zx}\cos\phi \end{pmatrix} e^{ikx}. \tag{S.20}$$

Now in Eq. (S.4), we are allowed to take spatial averaging in z under the thin film approximation. For wires, we also average over the wire width by integrating over x. For films, we instead decompose it into the Fourier components labelled by k. These operations eliminate all the spatial dependences (Eq. (S.7) is in fact valid only after these operations), yielding

$$\begin{pmatrix} -H_\parallel & i\omega/\mu_0|\gamma| \\ -i\omega/\mu_0|\gamma| & -H_\perp \end{pmatrix}\begin{pmatrix} n_\parallel \\ n_\perp \end{pmatrix} = -\frac{\gamma}{|\gamma|}\boldsymbol{h} + \frac{1}{\mu_0 M_s}\sum_{\mu}^{(k\text{ fixed for films})}\begin{pmatrix} a_\mu \\ b_\mu \end{pmatrix}\beta_\mu, \tag{S.21}$$

where the effective coupling constants a_μ, b_μ for each mode μ are defined by

$$a_\mu = \frac{1}{d}\int_{-d/2}^{d/2} dz\left[-2b_1\epsilon^{\mu}_{xx}\cos\phi\sin\phi + \left\{2b_2\epsilon^{\mu}_{xy} - (1-N_\perp)\,\omega^{\mu}_{xy}\right\}\left(\cos^2\phi - \sin^2\phi\right)\right] \times \begin{cases} 1 & \text{film} \\ \text{sinc}\,(kw/2) & \text{wire} \end{cases}, \tag{S.22}$$

$$b_\mu = \frac{1}{d}\int_{-d/2}^{d/2} dz\left\{2b_2\left(\epsilon^{\mu}_{zx}\cos\phi + \epsilon^{\mu}_{zy}\sin\phi\right) - N_\perp\omega^{\mu}_{zy}\sin\phi - (2N_\perp - 1)\,\omega^{\mu}_{zx}\cos\phi\right\} \times \begin{cases} 1 & \text{film} \\ \text{sinc}\,(kw/2) & \text{wire} \end{cases}. \tag{S.23}$$

Note that $a_{R,k}, b_{R,k}$ are in general larger by a factor of $\sqrt{|k|\,L_z}$ than $a_{(P,S,T),k,k_z}, b_{(P,S,T),k,k_z}$ due to the normalisation constants (S.19). This occurs due to the fact that the relative weight of the acoustic wave overlapping with the magnetic film is much greater for the surface modes than for the bulk modes. It motivates us to neglect the couplings to the bulk modes, which is ultimately justified by the results of the numerical simulations.

The mode decomposition of Eq. (S.5) is carried out by multiplying it by $\boldsymbol{v}^{\dagger}_{\mu}e^{-ikx}$ from left and integrate over the the whole volume $-L_x/2 < x < L_x/2, -L_z - d/2 < z < d/2$. Using the orthonormality of the mode functions, only the term proportional to β_μ survives on the left-hand-side. On the right-hand-side, noting $n_{\parallel,\perp}$ are nonzero only inside the region occupied by the magnet $-w/2 < x < w/2, -d/2 < z < d/2$, we obtain

$$\begin{aligned}
&\frac{1}{L_x}\int_{-L_x/2}^{L_x/2} dx\frac{1}{L_z}\int_{-L_z-d/2}^{d/2} dz\,\boldsymbol{v}^{\dagger}_{\mu}\cdot\boldsymbol{f}_{\text{eff}}e^{-ikx} \\
&= \frac{1}{L_x}\int_{-w/2}^{w/2} dx\frac{e^{-ikx}}{L_z}\int_{-d/2}^{d/2} dz\,\boldsymbol{v}^{\dagger}_{\mu}\cdot\left[\hat{\partial}_x\begin{pmatrix} -2b_1 n_\parallel\cos\phi\sin\phi \\ \left\{b_2 + \mu_0 M_s^2\,(1-N_\perp)/2\right\}n_\parallel\left(\cos^2\phi - \sin^2\phi\right) \\ \left\{b_2 - \mu_0 M_s^2\,(2N_\perp - 1)/2\right\}n_\perp\cos\phi \end{pmatrix} + \hat{\partial}_z\begin{pmatrix} \left\{b_2 + \mu_0 M_s^2\,(2N_\perp - 1)/2\right\}\cos\phi \\ \left(b_2 + \mu_0 M_s^2 N_\perp/2\right)\sin\phi \\ 0 \end{pmatrix} n_\perp\right] \\
&= -\frac{1}{L_x}\int_{-w/2}^{w/2} dx\frac{1}{L_z}\int_{-d/2}^{d/2} dz\left\{\partial_x\left(\boldsymbol{v}^{\dagger}_{\mu}e^{-ikx}\right)\right\}\cdot\begin{pmatrix} -2b_1 n_\parallel\cos\phi\sin\phi \\ \left\{b_2 + \mu_0 M_s^2\,(1-N_\perp)/2\right\}n_\parallel\left(\cos^2\phi - \sin^2\phi\right) \\ \left\{b_2 - \mu_0 M_s^2\,(2N_\perp - 1)/2\right\}n_\perp\cos\phi \end{pmatrix} \\
&\quad -\frac{1}{L_x}\int_{-w/2}^{w/2} dx\frac{1}{L_z}\int_{-d/2}^{d/2} dz\left\{\partial_z\left(\boldsymbol{v}^{\dagger}_{\mu}e^{-ikx}\right)\right\}\cdot\begin{pmatrix} \left\{b_2 + \mu_0 M_s^2\,(2N_\perp - 1)/2\right\}\cos\phi \\ \left(b_2 + \mu_0 M_s^2 N_\perp/2\right)\sin\phi \\ 0 \end{pmatrix} n_\perp \;=\; -\frac{w}{L_x}\frac{d}{L_z}\left(\overline{a_\mu}n_\parallel + \overline{b_\mu}n_\perp\right).
\end{aligned} \tag{S.24}$$

Note that in the second equality, were it not for the boundary delta functions in $\hat{\partial_{x,z}}$, we would have had additional surface terms, and consequently the result could not have been written solely in terms of a_μ, b_μ. Therefore, Eq. (S.5) reduces to

$$\rho\left(\omega^2 - \omega_\mu^2 + i\frac{\omega}{\tau}\right)\beta_\mu = -f_\mu + \frac{w}{L_x}\frac{d}{L_z}\left(\overline{a_\mu}n_\parallel + \overline{b_\mu}n_\perp\right), \quad f_\mu = \frac{1}{L_x}\int_{-L_x/2}^{L_x/2} dx\frac{1}{L_z}\int_{-d/2}^{d/2} dz\,\boldsymbol{v}^{\dagger}_{\mu}\cdot\boldsymbol{f}e^{-ikx}, \tag{S.25}$$

where the mode frequency ω_μ is given by $\omega^2_{P,k,k_z} = c_P^2\left(k^2 + k_z^2\right), \omega^2_{(S,T),k,k_z} = c_S^2\left(k^2 + k_z^2\right), \omega^2_{R,k} = c_R^2 k^2$, and the acoustic damping $1/\tau$ has been added by hand. Retaining only the surface mode and specialising in the film geometry, we derive Eq. (3) in the main text.

III. RAYLEIGH SAW AMPLITUDE

For the film geometry, by discarding the bulk acoustic waves, the problem reduces to that of one spin wave mode and one acoustic wave mode with a common wavenumber k:

$$\begin{pmatrix} n_\parallel \\ n_\perp \\ \beta_{R,k} \end{pmatrix} = -\chi_k(\omega) \begin{pmatrix} (\gamma/|\gamma|)h_k^\parallel \\ (\gamma/|\gamma|)h_k^\perp \\ f_{R,k} \end{pmatrix}, \quad \chi_k(\omega) = \begin{pmatrix} -H_\parallel + i\alpha\omega/\mu_0|\gamma| & i\omega/\mu_0|\gamma| & -a_{R,k}/\mu_0 M_s \\ -i\omega/\mu_0|\gamma| & -H_\perp + i\alpha\omega/\mu_0|\gamma| & -b_{R,k}/\mu_0 M_s \\ -d\overline{a_{R,k}}/L_z & -d\overline{b_{R,k}}/L_z & \rho\left(\omega^2 - c_R^2 k^2 + i\omega/\tau\right) \end{pmatrix}^{-1}. \tag{S.26}$$

Note that we used a different notation for the coupling constants $a_{R,k} = g_\parallel \cos\phi, b_{R,k} = g_\perp \cos\phi$ in the main text, primarily to tidy up the notations and facilitate the angular dependence analysis. We are interested in the amplitude of the Rayleigh SAW $\beta_{R,k}$ generated by some external magnetic fields $h_k^{\parallel,\perp}$ or mechanical forces $f_{R,k}$. Since the generalised susceptibility matrix is 3-by-3, it can be readily computed. We obtain

$$\begin{aligned} \det\chi_k(\omega) \begin{pmatrix} n_\parallel \\ n_\perp \\ \beta_{R,k} \end{pmatrix} &= \begin{pmatrix} \left\{(H_\perp - i\alpha\omega/\mu_0|\gamma|)\, h_k^\parallel + (i\omega/\mu_0|\gamma|)h_k^\perp\right\}\rho\left(\omega^2 - c_R^2k^2 + i\omega/\tau\right)\gamma/|\gamma| \\ \left\{(H_\parallel - i\alpha\omega/\mu_0|\gamma|)\, h_k^\perp - (i\omega/\mu_0|\gamma|)h_k^\parallel\right\}\rho\left(\omega^2 - c_R^2k^2 + i\omega/\tau\right)\gamma/|\gamma| \\ \left\{\left(1+\alpha^2\right)\omega^2/\mu_0^2\gamma^2 - H_\parallel H_\perp + i\left(H_\parallel + H_\perp\right)\alpha\omega/\mu_0|\gamma|\right\} f_{R,k} \end{pmatrix} \\ &+ \begin{pmatrix} d\left|b_{R,k}\right|^2/L_z\mu_0 M_s & -d\overline{b_{R,k}}a_{R,k}/L_z\mu_0 M_s & \frac{1}{\mu_0 M_s}\left\{\left(H_\perp - \frac{i\alpha\omega}{\mu_0|\gamma|}\right)a_{R,k} + \frac{i\omega b_{R,k}}{\mu_0|\gamma|}\right\} \\ -d\overline{a_{R,k}}b_{R,k}/L_z\mu_0 M_s & d\left|a_{R,k}\right|^2/L_z\mu_0 M_s & \frac{-1}{\mu_0 M_s}\left\{\left(H_\parallel - \frac{i\alpha\omega}{\mu_0|\gamma|}\right)b_{R,k} - \frac{i\omega}{\mu_0|\gamma|}a_{R,k}\right\} \\ \frac{d}{L_z}\left\{\left(H_\perp - \frac{i\alpha\omega}{\mu_0|\gamma|}\right)\overline{a_{R,k}} - \frac{i\omega}{\mu_0|\gamma|}\overline{b_{R,k}}\right\} & -\frac{d}{L_z}\left\{\left(H_\parallel - \frac{i\alpha\omega}{\mu_0|\gamma|}\right)\overline{b_{R,k}} - \frac{i\omega}{\mu_0|\gamma|}\overline{a_{R,k}}\right\} & 0 \end{pmatrix} \begin{pmatrix} \gamma h_k^\parallel/|\gamma| \\ \gamma h_k^\perp/|\gamma| \\ f_{R,k} \end{pmatrix}, \end{aligned} \tag{S.27}$$

where

$$\begin{aligned} \frac{1}{\det\chi_k(\omega)} &= \rho\left\{H_\parallel H_\perp - \left(1+\alpha^2\right)\frac{\omega^2}{\mu_0^2\gamma^2} - \left(H_\parallel + H_\perp\right)\frac{i\alpha\omega}{\mu_0|\gamma|}\right\}\left(\omega^2 - c_R^2k^2 + i\frac{\omega}{\tau}\right) \\ &+ \frac{d}{L_z}\frac{1}{\mu_0 M_s}\left\{\left(H_\perp - \frac{i\alpha\omega}{\mu_0|\gamma|}\right)\left|a_{R,k}\right|^2 + \left(H_\parallel - \frac{i\alpha\omega}{\mu_0|\gamma|}\right)\left|b_{R,k}\right|^2 + \frac{i\omega}{\mu_0|\gamma|}\left(\overline{a_{R,k}}b_{R,k} - \overline{b_{R,k}}a_{R,k}\right)\right\}. \end{aligned} \tag{S.28}$$

Setting $f_{R,k} = 0$ yields Eq. (6) of the main text.

In the wire geometry, the problem does not reduce to a 3-by-3 matrix inversion since the Kittel mode couples to multiple Rayleigh SAW modes with k in the range of roughly $|k| \lesssim 2\pi/w$. Nevertheless, the response of the system against a purely magnetic driving, i.e. $f_{R,k} = 0$, is still computable analytically. For this purpose, we introduce the vector notation $\boldsymbol{\beta}_R = (\beta_{R,k_1}, \beta_{R,k_2}, \cdots)^T, \boldsymbol{a}_R = (a_{R,k_1}, a_{R,k_2}, \cdots), \boldsymbol{b}_R = (b_{R,k_1}, b_{R,k_2}, \cdots)$. The linearised equations of motion (S.4), (S.5) under the mode expansion for the wire geometry are written as

$$\begin{pmatrix} n_\parallel \\ n_\perp \\ \boldsymbol{\beta}_R \end{pmatrix} = -\frac{\gamma}{|\gamma|}\begin{pmatrix} -H_\parallel + i\alpha\omega/\mu_0|\gamma| & i\omega/\mu_0|\gamma| & -\boldsymbol{a}_R/\mu_0 M_s \\ -i\omega/\mu_0|\gamma| & -H_\perp + i\alpha\omega/\mu_0|\gamma| & -\boldsymbol{b}_R/\mu_0 M_s \\ -wd\boldsymbol{a}_R^\dagger/L_xL_z & -wd\boldsymbol{b}_R^\dagger/L_xL_z & G(\omega)^{-1} \end{pmatrix}^{-1}\begin{pmatrix} h^\parallel \\ h^\perp \\ 0 \end{pmatrix}, \tag{S.29}$$

where

$$G(\omega)^{-1} = \rho\begin{pmatrix} \omega^2 - c_R^2k_1^2 + i\omega/\tau & 0 & \cdots \\ 0 & \omega^2 - c_R^2k_2^2 + i\omega/\tau & \ddots \\ \vdots & \ddots & \ddots \end{pmatrix}. \tag{S.30}$$

The inverse yields

$$\begin{pmatrix} n_\parallel \\ n_\perp \end{pmatrix} = -\frac{\gamma}{|\gamma|}\left\{\begin{pmatrix} -H_\parallel + i\alpha\omega/\mu_0|\gamma| & i\omega/\mu_0|\gamma| \\ -i\omega/\mu_0|\gamma| & -H_\perp + i\alpha\omega/\mu_0|\gamma| \end{pmatrix} - \frac{wd}{L_xL_z}\frac{1}{\mu_0 M_s}\begin{pmatrix} \boldsymbol{a}_R G(\omega)\boldsymbol{a}_R^\dagger & \boldsymbol{a}_R G(\omega)\boldsymbol{b}_R^\dagger \\ \boldsymbol{b}_R G(\omega)\boldsymbol{a}_R^\dagger & \boldsymbol{b}_R G(\omega)\boldsymbol{b}_R^\dagger \end{pmatrix}\right\}^{-1}\begin{pmatrix} h^\parallel \\ h^\perp \end{pmatrix}, \tag{S.31}$$

$$\boldsymbol{\beta}_R = -\frac{wd}{L_xL_z}G(\omega)\left(\boldsymbol{a}_R^\dagger n_\parallel + \boldsymbol{b}_R^\dagger n_\perp\right) \quad \Rightarrow \quad \beta_{R,k} = -\frac{wd}{L_xL_z}\frac{1}{\rho}\frac{\overline{a_{R,k}}n_\parallel + \overline{b_{R,k}}n_\perp}{\omega^2 - c_R^2k^2 + i\omega/\tau}. \tag{S.32}$$

Note that the second term in the curly braces in Eq. (S.31) can be considered a self-energy for the Kittel mode arising from the coupling to the Rayleigh SAWs, which can be computed by evaluating the summation over k:

$$\begin{pmatrix} \boldsymbol{a}_R G(\omega)\boldsymbol{a}_R^\dagger & \boldsymbol{a}_R G(\omega)\boldsymbol{b}_R^\dagger \\ \boldsymbol{b}_R G(\omega)\boldsymbol{a}_R^\dagger & \boldsymbol{b}_R G(\omega)\boldsymbol{b}_R^\dagger \end{pmatrix} = \frac{1}{\rho}\sum_k \frac{1}{\omega^2 - c_R^2k^2 + i\omega/\tau}\begin{pmatrix} \left|a_{R,k}\right|^2 & a_{R,k}\overline{b_{R,k}} \\ b_{R,k}\overline{a_{R,k}} & \left|b_{R,k}\right|^2 \end{pmatrix}. \tag{S.33}$$

The net effects of the self-energy are to shift the Kittel mode resonance frequency and to broaden the resonance, but only by a small amount proportional to $w/L_x \ll 1$. Note that another small factor d/L_z is compensated by the factor $|k|L_z$ arising from the normalisation constant N_R in $a_{R,k}, b_{R,k}$. Hence, we can ignore the self-energy in the leading order approximation, and obtain

$$\begin{aligned}\beta_{R,k} \approx -\frac{\gamma}{|\gamma|}\frac{wd}{L_x L_z}\left[\rho\left(\omega^2 - c_R^2 k^2 + i\omega/\tau\right)\left\{H_\parallel H_\perp - \left(1+\alpha^2\right)\frac{\omega^2}{\mu_0^2\gamma^2} - i\left(H_\parallel + H_\perp\right)\frac{\alpha\omega}{\mu_0|\gamma|}\right\}\right]^{-1} \\ \times\left[\left\{\left(H_\perp - \frac{i\alpha\omega}{\mu_0|\gamma|}\right)\overline{a_{R,k}} - \frac{i\omega}{\mu_0|\gamma|}\overline{b_{R,k}}\right\}h^\parallel + \left\{\left(H_\parallel - \frac{i\alpha\omega}{\mu_0|\gamma|}\right)\overline{b_{R,k}} + \frac{i\omega}{\mu_0|\gamma|}\overline{a_{R,k}}\right\}h^\perp\right],\end{aligned} \tag{S.34}$$

which is identical to Eq. (6) in the main text for the film geometry, apart from the appearance of the factor w/L_x in the effective coupling constants $a_{R,k}, b_{R,k}$ and the overall amplitudes.

The total displacement field $\boldsymbol{u}$ is given by the sum over k: $\boldsymbol{u} = \sum_k \beta_{R,k}\boldsymbol{v}_{R,k}e^{ikx}$. To estimate the order of magnitude of the signal, we calculate $\boldsymbol{u}$ at the surface $z = d/2$, averaged over t and x:

$$|\boldsymbol{u}|^2 = \sum_k \left|\beta_{R,k}\right|^2\left|\boldsymbol{v}_{R,k}\right|^2 = \sum_k \left|\beta_{R,k}\right|^2\frac{\left(1-\xi_S^2\right)^2 + \left(1-\xi_P^2\right)}{|N_R|^2}\xi_S^4. \tag{S.35}$$

We can again observe that the dependence on L_z drops out by L_z^{-2} coming from the prefactor in Eq. (S.34) cancelling a factor of L_z from the squares of $a_{R,k}, b_{R,k}$ and another from $|N_R|^{-2}$. For the film geometry, only one value of k resonant at ω is important. Assuming the double resonance, we have

$$\beta_{R,k} \approx -\frac{\gamma}{|\gamma|}\frac{d}{L_z}\frac{\tau}{i\rho\omega}\frac{i\mu_0|\gamma|}{\alpha\omega\left(H_\parallel + H_\perp\right)}\left\{\left(H_\perp\overline{a_{R,k}} - \frac{i\omega}{\mu_0|\gamma|}\overline{b_{R,k}}\right)h^\parallel + \left(H_\parallel\overline{b_{R,k}} + \frac{i\omega}{\mu_0|\gamma|}\overline{a_{R,k}}\right)h^\perp\right\} \approx -\frac{d}{L_z}\frac{\tau}{\rho\omega}\frac{\mu_0\gamma}{\alpha\omega}\left(\overline{a_{R,k}} - i\overline{b_{R,k}}\right)\left(h_k^\parallel + ih_k^\perp\right). \tag{S.36}$$

Plugging in the numbers $|k| = 1.5\times10^7$ rad/m, $d = 50$ nm, $\rho\omega^2 = 5\times10^{24}$ J/m^5, $\omega/\mu_0|\gamma| = 2\times10^5$ A/m, $b_1 = 3.5\times10^5$ J/m^3, $b_2 = 2b_1$, we estimate

$$|\boldsymbol{u}|^2 \sim \left(\frac{\tau\omega}{\alpha}\right)^2\times10^{-24}\times\left(\frac{\left|h^\parallel + ih^\perp\right|}{10^5\mathrm{A/m}}\right)^2\ [\mathrm{m}^2]. \tag{S.37}$$

The prefactor comes form the resonant enhancement and can be as large as $\tau\omega/\alpha > 10^6$ for YIG/GGG heterostructures. The value of $\left|h_k^\parallel + ih_k^\perp\right|$ is limited by requiring the spin wave amplitude determined by Eq. (S.27) to remain in the linear regime $\left|n_\parallel, n_\perp\right| \lesssim 10^{-2}$. For $\alpha = 10^{-3}$, we need $\left|h_k^\parallel + ih_k^\perp\right| \lesssim 1$ A/m. This leads to the attainable mean square displacement of order 10 pm. Referring to Eq. (S.21), $\beta_\mu = 1$ pm translates to an effective magnetic field of order 10^{-4} A/m, which is sufficient to trigger a secondary spin wave resonance near the detector CPW in Fig. 2(b) in the main text. Note that a similar experiment of magnetic driving and detection of acoustic waves was successfully carried out in Ref. 8 in the main text, albeit in a different geometry. Therefore, we believe the SAWs generated by spin wave resonances are also detectable in a suitably designed experimental setup.

IV. NUMERICAL SIMULATION

We perform numerical simulations of the YIG/GGG heterostructures by COMSOL Multiphysics which solves partial differential equations based on finite elements method. The geometry for the simulations is plotted in Fig. S2 where the YIG film and GGG film are separately established and simulated in a 2D model (x-z plane) and the y direction is assumed to be uniform.

The dynamics of normalised magnetisation $\boldsymbol{m} = \boldsymbol{M}/M_s = (m_x, m_y, m_z)$ and the dynamics of lattice displacement vector

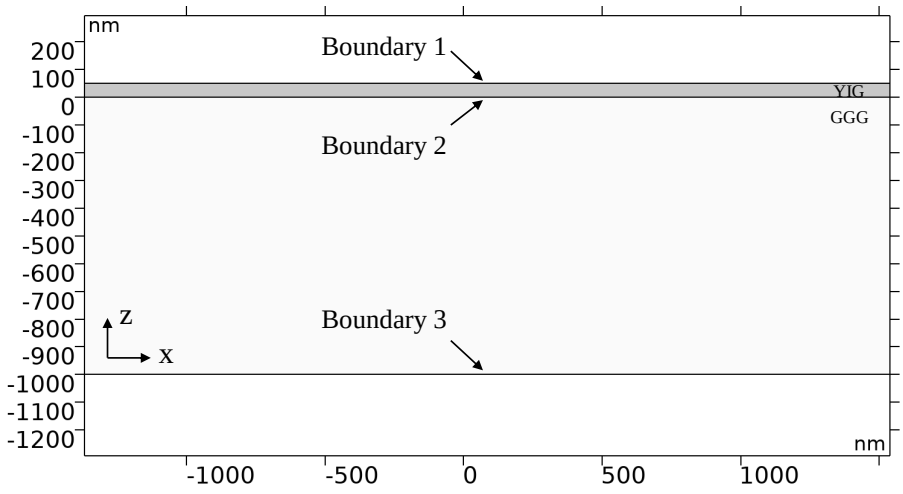

FIG. S2. Geometry of YIG/GGG heterostructures for numerical simulation. A magnetic YIG film with thickness 50mm is attached on the GGG substrate with thickness 1000mm.

$\boldsymbol{u} = (u_x, u_y, u_z)$ inside the YIG film are described by hybrid equations Eq. (S.38) with $\nabla = (\partial/\partial x, \partial/\partial z)$

$$
\begin{cases}
\dfrac{\partial m_x}{\partial t} = -\gamma(m_y H_z^{\text{eff}} - m_z H_y^{\text{eff}}) + \gamma\dfrac{2b_1}{\mu_0 M_s}\left(m_y m_z \dfrac{\partial u_z}{\partial z}\right) \\
\qquad\qquad + \gamma\dfrac{b_2}{\mu_0 M_s}\left[m_y^2\dfrac{\partial u_y}{\partial z} + m_x m_y\left(\dfrac{\partial u_z}{\partial x} + \dfrac{\partial u_x}{\partial z}\right) - m_z m_x\dfrac{\partial u_y}{\partial x} - m_z^2\dfrac{\partial u_y}{\partial z}\right], \\
\dfrac{\partial m_y}{\partial t} = -\gamma(m_z H_x^{\text{eff}} - m_x H_z^{\text{eff}}) + \gamma\dfrac{2b_1}{\mu_0 M_s}\left[m_z m_x\left(\dfrac{\partial u_x}{\partial x} - \dfrac{\partial u_z}{\partial z}\right)\right] \\
\qquad\qquad + \gamma\dfrac{b_2}{\mu_0 M_s}\left[m_y m_z\dfrac{\partial u_y}{\partial x} + m_z^2\left(\dfrac{\partial u_z}{\partial x} + \dfrac{\partial u_x}{\partial z}\right) - m_y m_x\dfrac{\partial u_y}{\partial z} - m_x^2\left(\dfrac{\partial u_z}{\partial x} + \dfrac{\partial u_x}{\partial z}\right)\right], \\
\dfrac{\partial m_z}{\partial t} = -\gamma(m_x H_y^{\text{eff}} - m_y H_x^{\text{eff}}) + \gamma\dfrac{2b_1}{\mu_0 M_s}\left[m_x m_y\left(-\dfrac{\partial u_x}{\partial x}\right)\right] \\
\qquad\qquad + \gamma\dfrac{b_2}{\mu_0 M_s}\left[m_x^2\dfrac{\partial u_y}{\partial x} + m_z m_x\dfrac{\partial u_y}{\partial z} - m_y^2\dfrac{\partial u_y}{\partial x} - m_z m_y\left(\dfrac{\partial u_z}{\partial x} + \dfrac{\partial u_x}{\partial z}\right)\right], \\
\rho_{\text{YIG}}\dfrac{\partial^2 u_x}{\partial t^2} + \eta\dfrac{\partial u_x}{\partial t} = \mu_{\text{YIG}}\nabla^2 u_x + (\lambda_{\text{YIG}} + \mu_{\text{YIG}})\left(\dfrac{\partial^2 u_x}{\partial x^2} + \dfrac{\partial^2 u_z}{\partial x \partial z}\right) + 2b_1 m_x\dfrac{\partial m_x}{\partial x} + b_2\left(\dfrac{\partial m_z}{\partial z}m_x + \dfrac{\partial m_x}{\partial z}m_z\right), \\
\rho_{\text{YIG}}\dfrac{\partial^2 u_y}{\partial t^2} + \eta\dfrac{\partial u_y}{\partial t} = \mu_{\text{YIG}}\nabla^2 u_y + b_2\left(\dfrac{\partial m_x}{\partial x}m_y + \dfrac{\partial m_y}{\partial x}m_x + \dfrac{\partial m_y}{\partial z}m_z + \dfrac{\partial m_z}{\partial z}m_y\right), \\
\rho_{\text{YIG}}\dfrac{\partial^2 u_z}{\partial t^2} + \eta\dfrac{\partial u_z}{\partial t} = \mu_{\text{YIG}}\nabla^2 u_z + (\lambda_{\text{YIG}} + \mu_{\text{YIG}})\left(\dfrac{\partial^2 u_x}{\partial z \partial x} + \dfrac{\partial^2 u_z}{\partial z^2}\right) + 2b_1 m_z\dfrac{\partial m_z}{\partial z} + b_2\left(\dfrac{\partial m_z}{\partial x}m_x + \dfrac{\partial m_x}{\partial x}m_z\right).
\end{cases}
\tag{S.38}
$$

Here the first three equations are Landau-Lifshitz-Gilbert equations in the presence of magneto-elastic coupling. The effective field $\boldsymbol{H}^{\text{eff}} = (H_x^{\text{eff}}, H_y^{\text{eff}}, H_z^{\text{eff}}) = A\nabla^2\boldsymbol{m} - M_s m_z\hat{\boldsymbol{z}} + H\cos\theta\,\hat{\boldsymbol{x}} + H\sin\theta\,\hat{\boldsymbol{y}} + \boldsymbol{h}_{\text{ext}}$ includes exchange interaction, effective hard-axis anisotropy induced by demagnetising field, static external magnetic field with in-plane angle θ and excitation field for generating spin waves. The last three equations of Eq. S.38 are the equations of motion for elastic waves, where ρ is the mass density and μ, λ are Lamé constants. The velocities of elastic waves are determined by Lamé constants with the relations $c_P = \sqrt{(2\mu + \lambda)/\rho}$ and $c_S = \sqrt{\mu/\rho}$. The damping of elastic waves is taken into account phenomenologically via the friction term $\eta\partial\boldsymbol{u}/\partial t$. Since there is no magnetisation in the GGG substrate, the dynamics of elastic waves is governed by the equations of motion without

magnetic forces

$$\begin{cases} \rho_{\mathrm{GGG}} \dfrac{\partial^2 u_x}{\partial t^2} + \eta \dfrac{\partial u_x}{\partial t} = \mu_{\mathrm{GGG}} \nabla^2 u_x + (\lambda_{\mathrm{GGG}} + \mu_{\mathrm{GGG}}) \left(\dfrac{\partial^2 u_x}{\partial x^2} + \dfrac{\partial^2 u_z}{\partial x \partial z} \right), \\ \rho_{\mathrm{GGG}} \dfrac{\partial^2 u_y}{\partial t^2} + \eta \dfrac{\partial u_y}{\partial t} = \mu_{\mathrm{GGG}} \nabla^2 u_y, \\ \rho_{\mathrm{GGG}} \dfrac{\partial^2 u_z}{\partial t^2} + \eta \dfrac{\partial u_z}{\partial t} = \mu_{\mathrm{GGG}} \nabla^2 u_z + (\lambda_{\mathrm{GGG}} + \mu_{\mathrm{GGG}}) \left(\dfrac{\partial^2 u_x}{\partial z \partial x} + \dfrac{\partial^2 u_z}{\partial z^2} \right). \end{cases} \tag{S.39}$$

Due to the presence of magnetisation inside the YIG film, extra force terms are required on the boundary 1 and 2 respectively,

$$\boldsymbol{f} = \begin{pmatrix} \mp b_2 m_x m_z \\ \mp b_2 m_y m_z \\ \mp b_1 m_z^2 \end{pmatrix}, \quad - \text{ for boundary 1 and + for boundary 2.} \tag{S.40}$$

The inclusion of these boundary forces corresponds to the delta function in Eq. (S.9) in the analytical formalism above. The free-surfacel boundary condition is applied on the top surface (boundary 1 in Fig. S2). The lattice displacement on the bottom boundary (boundary 3 in Fig. S2) is constrained with $\boldsymbol{u} = 0$. Regions $x > 1000$ nm, $x < -1000$ nm and $x < -500$ nm are manually set as high-damping regions with $\eta = 5 \times 10^{14}$ N·s/m^4 and $\alpha = 0.2$ to avoid wave reflections from the boundaries.

In the numerical simulation, we apply a magnetic field pulse at the central region of the magnetic film (width 50 nm) $\boldsymbol{h}_{\mathrm{ext}} = 10[\mathrm{mT}] \sin(2\pi f_0 t)\hat{\boldsymbol{z}}$ with duration $t = 1/f_0$ and $f_0 = 5$ GHz is the Kittel mode frequency. The elastic waves are generated due to the magneto-elastic coupling and the signals $\sqrt{u_x^2 + u_z^2}$ are extracted at the coordinates $(x, z) = (\pm 900, 0)$ nm and are integrated over time for 1ns, representing the transmission intensity. The angular dependence of transmission is plotted in Fig. S3 where the in-plane angle θ is swept from 0 to 180 degrees. It can be seen that the transmission is reciprocal when $\theta = 0$ and $\theta = \pi$, while it demonstrates maximum non-reciprocity at $\theta \sim 0.36$. The signals do not reach zero at the angles of maximum non-reciprocity presumably because of the bulk elastic waves induced by the pulse, which are neglected in the analytical calculations.

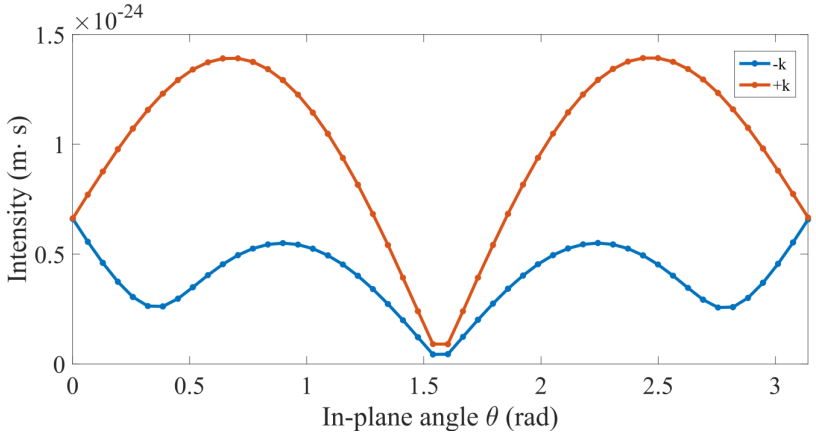

FIG. S3. Angular dependence of SAW transmission intensity integrated in time for 1 ns. The blue (red) curve is for -k (+k) case.